Ruff SW, Christensen PR (2002) Bright and dark regions on Mars: particle size and mineralogical characteristics based on thermal emission spectrometer data. J Geophys Res 107(E12):5127. doi:10.1029/2001JE001580

Schenk P, Hamilton DP, Johnson RE, McKinnon WB, Paranicas C, Schmist J, Showalter MR (2011) Plasma, plumes and rings: Saturn system dynamics as recorded in global color patterns on its midsize icy satellites. Icarus 211:740–757

See TJJ (1910) On the craters, mountains, Maria and other phenomena observed on the surface of the Moon, and on the indicated processes of planetary growth. In: Researches on the evolution of the stellar systems. II: the capture theory of cosmical evolution. Thos. P. Nichols, Lynn, Mas https://archive.org/details/researchesonevol02seetuoft

Soter S (1974) IAU colloquium 28, Cornell University. Cited by Tamayo et al. (2011)

Spencer JR, Calvin WM, Person MJ (1995) Charge-coupled-device spectra of the Galilean satellites: molecular oxygen on Ganymede. J Geophys Res 100:19049–19056

Tamayo D, Burns JA, Hamilton DP, Hedman MM (2011) Finding the trigger to Iapetus' odd global albedo pattern: dynamics of dust from Saturn's irregular satellites. Icarus 215:260–278

Albedo Feature

Péter Kardeván[1], Henrik Hargitai[2], Angelo Zinzi[3] and Francesca Esposito[4]
[1]retired from Department of Environmental Geology, Geological and Geophysical Institute of Hungary, Budapest, Hungary
[2]NASA Ames Research Center, Moffett Field, CA, USA
[3]ASI Science Data Center / INAF - Osservatorio Astronomico di Roma, Rome, Italy
[4]INAF-Osservatorio Astronomico di Capodimonte, Naples, Italy

Definition

An albedo feature is a region on the surface of a nonluminous celestial body (e.g., planet, moon, or small body) with distinct brightness (radiance) values or color, i.e., exhibiting observable/measurable brightness- or color-contrast relative to its surroundings. Albedo features were traditionally identified by doing spectrally integrated observation of the reflected sunlight with a telescope in the visible spectrum range of light and having adequate spatial resolution to resolve distinct parts of the surface of the object. Detection of the brightness variations is today extended to photometric (radiometric) measurements with modern satellite/spacecraft spectrophotometers or spectroradiometers at separate monochromatic wavelengths or integrated observations in other wavelength regions as well (see *spectral albedo, narrowband albedo*, *and broadband albedo*). Albedo features result from those brightness variations, that are due to variations of the reflective properties (often referred to as albedo) of a planetary surface.

Variants

Albedo pattern, albedo marking.

IAU Definition

Geographic area distinguished by amount of reflected light (IAU Gazetteer 2014).

Identification

The identification and mapping of albedo features are achieved through observations of the relative brightness variations of the planetary surfaces that can be carried out either by photographic methods (analog photoplates or digital photographs), photometric (radiometric) spot measurements and recording digital images by imaging photometers, spectrophotometers, or spectroradiometers.

The delineation of albedo features on panchromatic or monochromatic photography is based on the creation of photographic isodensity contours (analog films) or isophotic contours (digital images) separating different categories of gray levels of the image. Special terminology has been developed for making standard reference to the different gray levels of distinguished albedo features (see "Classification of Albedo Categories"). Since these photographic density-based brightness scales are in nonlinear

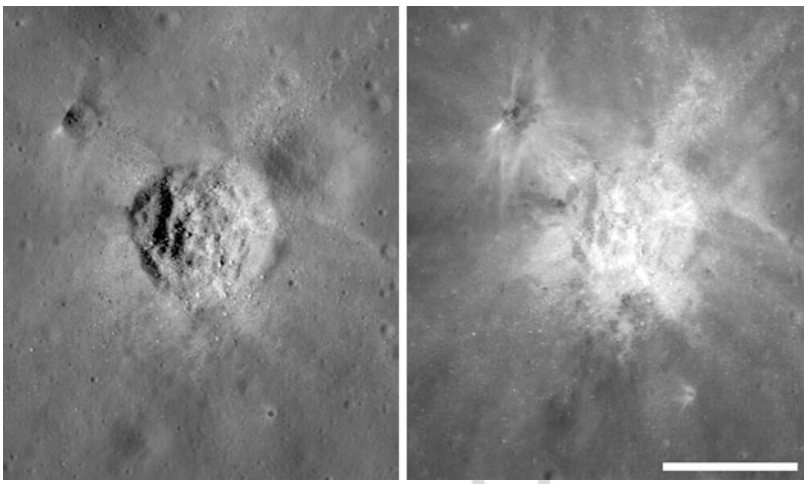

Albedo Feature, Fig. 1 This image pair illustrates the effects of illumination, or phase angle, in recognizing different aspects of the same feature (a 200 m diameter crater) on the lunar surface (Plescia 2009). *Left*: M1046700 19L: incidence angle 50° (low sun), *right*: M1070 35386L incidence angle 25° (high sun). Scale bar 200 m. LROC Narrow Angle Camera, PIA12916 (NASA/GSFC/ASU)

functional relationship with the brightness or albedo defined in photometry (radiometry) (see "Concept of Albedo"), the term relative albedo contrast is used in such cases, and in all other ones, when arbitrary scales are used often specific to the authors or to the research project. The photogeological interpretation calls however for labeling the delineated albedo feature with the albedo values themselves that conform to its photometrical definition. Therefore, photometric (radiometric) calibration is carried out. Albedo value ranges from 0 (blackbody) to 1 (ideal reflector). During classification, typically only few subtypes are defined: high albedo (bright), intermediate, and low albedo (dark) (if needed, also very high and/or very low). The general term "albedo" in many photogeologic studies refers to relative, snow- or frost-free surface albedo (Prockter et al. 1998).

The term "albedo feature" is used in connection with spatial variation of surface brightness and called sometimes interchangeably as albedo markings or albedo patterns.

The term albedo pattern, however, can be used in connection with characteristic time variation of albedo in the sense of signatures of certain surface/atmospheric processes.

Albedo features can be permanent or variable. Sagan et al. (1972) defined *variable features* as variable, snow-/frost-free land albedo patterns that change with time (Sagan et al. 1972) (► dark deposits (Mars) and ► wind streak).

The albedo patterns in a terrestrial environment correspond to different surface cover classes (vegetation, soil, etc.) having decisive role in climate forcing, and their reflective properties can be measured by satellite-, airborne-, or field-measuring systems.

Albedo features may or may not correspond to relief features; albedo features may not show any topography (e.g., albedo patterns such as ► swirls or ► dust devil tracks).

Albedo patterns are best visible at high sun (e.g., near full Moon). In contrast, relief features are highlighted at low solar altitude angle (high incidence angle) (near the terminator line) where shadows are the longest and emphasize topography (Figs. 1 and 2).

The Concepts of Albedo

There are several types of albedo concept (often referred as albedo products) used in different branches of science such as astronomy, remote sensing of Earth, climatology and oceanography, etc. The detailed mapping of albedo features not only serves the purposes of planetary geology, but plays important role in the research of climate change of the Earth.

Different attributes (often more than one) are therefore attached to the term "albedo" to borrow specific meaning to it, establishing, thus, a precise terminology and making the plain term

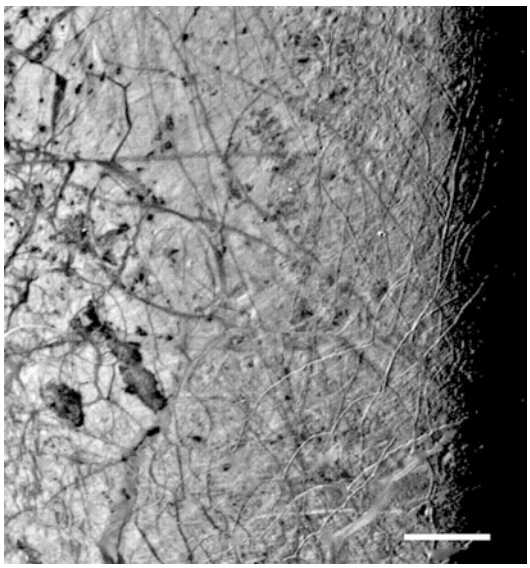

Albedo Feature, Fig. 2 Lineaments of the Jovian moon Europa "transform" from albedo features (seen under high solar altitude angle/low incidence angle) into topographic features (ridges) (observed in low sun conditions, near the terminator) (Lucchitta et al. 1981). Scale bar ca. 100 km. Voyager 2, PIA01504 (NASA/JPL)

"albedo" ambiguous. Yet, the definition of albedo, as an instruction of measurement, is general and commonly applicable in all specific albedo concepts.

Definitions of Albedo

According to a commonly accepted formulation, "Albedo is defined as the ratio of reflected solar shortwave radiation from a surface to that incident upon it" (Strugnell and Lucht 2001). Reflected radiation in the whole solar spectrum is referred namely as **shortwave radiation** (0.3–5.0 μm). This type of **broadband albedo** governs the amount of shortwave radiation that is effectively absorbed by the material of which a surface element is composed (Dumont et al. 2011). While broadband albedo products (also **bolometric albedo of a celestial body** referring to the whole solar spectrum) are used rather in climatology and astronomy, planetary geological interpretation of **brightness variations** can be carried out by using **narrowband albedo** or **spectral albedo** products.

The definition of albedo given above implies that the quantification of the incident and reflected radiation power can be made either locally, using **surface densities of radiation power**, or globally, characterizing the incoming radiation power over the whole surface using surface-integrated values of surface densities, that is, the **radiation power values** themselves.

The albedo of a celestial body as a whole is used in planetology and astronomy or even in calibration procedures of the brightness values belonging to albedo features as well. One may find two versions of such albedo products with their surfaces modeled either as a plain disk or a sphere. Careful distinction should therefore be made, when using those types of albedo integrated to the whole surface of a celestial body, between **bond albedo** also known as **spherical albedo** and the **geometric albedo** also known as **physical albedo**. Also, distinction between the brightness concepts of a celestial body and that of a surface should be made. The former is in functional connection to the **magnitude of a star** and the latter being synonym of the term **specific intensity** or **radiance**.

The mapping of albedo features applies the local characterization, i.e., **surface densities of radiation power** having the physical dimension of electromagnetic power/m^2. Thus, the term "albedo" that is used in connection with albedo features is defined as a **characteristic reflective quality of a surface element** modeled locally as plain surface. These special albedo products are called sometimes **material albedo** or **inherent albedo** in planetology, indicating that it is an **intrinsic property** of the surface element that can be referred in remote sensing unambiguously as **true intrinsic surface albedo**.

The terminology of the radiometrical quantities used in terrestrial environments is quite different, because both incident and reflected radiation power can be measured on the Earth's surface. Therefore, a more specific definition has been accepted: "Albedo at some level of a geophysical system is defined as the ratio between the upward flux density . . . exiting that particular

level and the downward flux density impinging on that same level" (Pinty et al. 2005). This definition incorporates the term **surface albedo** again, as that measured at the bottom of atmosphere, i.e., at the level of the Earth's surface, seemingly in a different meaning as defined formerly in connection with albedo features in planetology. The problem is that in this case surface albedo is not an intrinsic feature of the surface. It is referred therefore as **apparent surface albedo**, contrary to **intrinsic surface albedo** that can be calculated in terrestrial environment by modeling of atmospheric radiation transfer (Liang et al. 1999) (also see below). The "geophysical system" means here a complex system of an unisotropically scattering surface with arbitrary topography and the consequent shadow casting and mutual view shadowing that is coupled with an inhomogeneous atmosphere of changing composition above it scattering both upward and downward radiation anisotropically as well. Therefore, the measured surface albedo depends on the spectral and angular distribution of both incident and reflected radiation power. Coupling of surface and atmosphere is incorporated by multiple scattering, which is often neglected in several albedo products (e.g., blue-sky albedo, etc.). This definition is special inasmuch as the power density is referred as **flux density**, and no distinction is made to the **irradiance** or **exitance** (Coakley 2002). This is acceptable only in the case of directional radiation component when photons travel in a single direction.

The diversity of albedo products arises even from the fact that the nature of radiation is different for **directional** and **diffuse radiation**. In the former case, the amount of radiation power arriving at a unit surface element is referred as **flux density**, and the radiation power is simply the surface integral of the flux density. Flux and irradiance concepts lead to the same value of these physical quantities in this case, as radiation arrives from a single direction. The same is true for reflected radiation in the case of **specular reflection**. The term "flux" is used, therefore, in planetology and in all other cases when the sole incoming radiation component is Sun's radiation that can well be modeled as a unidirectional one. However, in the case of diffuse radiation resulting from scattering by the surface and the atmosphere above it, the **surface density of radiation power** having though the same physical dimension as **flux density** is referred rather as **irradiance** or **exitance**, depending on whether incoming or reflected diffuse radiation is characterized, and the radiation power is a double integral of the surface and solid angle. In lighting industry, "albedo" is defined simply as **diffuse reflectance**, and in oceanography, the quotient of exitance/irradiance is used as albedo, corresponding to the definition by measurement instruction.

The intrinsic reflective feature of a surface is referred in **radiometry** either as **reflectivity** or **reflectance**, although the former term is used in modern terminology rather in connection with **specular reflections** (**Fresnel reflectivity**) depending solely on material parameters and the optical constants of participating media, and the latter is used rather in connection with scattering when a surface and a medium reflects/transmits radiation diffusively. The amount of reflected radiation depends also on the physical parameters (such as particle size, density, porosity, etc.) describing the inner structure of the surface material.

Planetary surfaces can be modeled either using single or multiple scattering models (Hapke 2012).

Broadband measuring instruments include pyrheliometers (for direct solar radiation), pyranometers, and photometers (for direct plus diffuse radiation in the visible wavelength range), while spectroradiometers (spectrophotometers) are used for **spectral measurements** resulting in different kinds of data as a consequence of their differently specified measuring parameters. These differences are discussed under the term **parameters of radiation geometry** including illumination and viewing geometry, which comprise angles "i" and "e" of incident and reflected radiation, the phase angle "g" (Fig. 3), and the solid angles "Ω", a measure of the collimation of radiation (not represented in Fig. 3). The types of reflectance according to different radiation geometry are best summarized by Hapke (2012) as

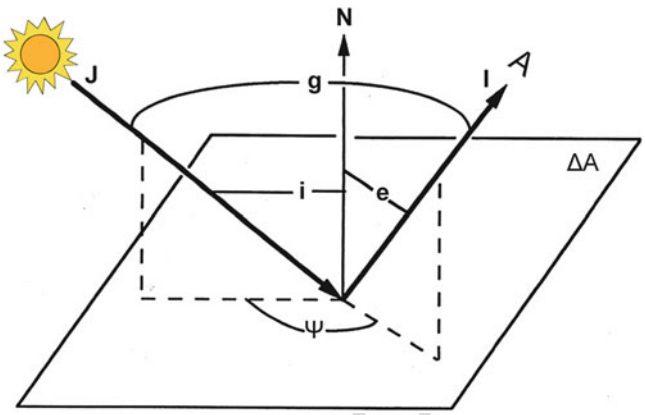

Albedo Feature, Fig. 3 Radiance I from a surface element ΔA. Incident (**i**), emission (**e**), and phase angles (**g**) are shown. J: irradiance (After Fig. 8 from Hapke (2012))

follows: in the modern usage (Nicodemus et al. 1977), the word "reflectance" is preceded by two adjectives, the first describing the degree of collimation of the illumination source and the second that of the detector, thus characterizing the differences in solid angles or beam geometries. **The term "reflectance"** of a surface is used here just as being the quotient of the reflected to incoming radiation power. The usual adjectives are "directional" (denoted by index "d"), "conical," or "hemispherical" (denoted by the index of "h"). For example, the directional-hemispherical reflectance, r_{dh}, is the total fraction of light scattered into the upward hemisphere by a surface illuminated from above by highly collimated source.

Current mathematical tools for specifying the anisotropic behavior of the diffuse reflection process in the presence of anisotropic diffuse illumination for different radiation geometries are based on the concepts of **radiance** and **the Bidirectional Reflectance Distribution Function (BRDF)**, incorporating both direct and diffuse radiation (Nicodemus et al. 1977). The instantaneous BRDF is a theoretical **kernel function** connecting incoming and reflected radiance that can only be modeled/estimated (not measured). The **multi-angle (directional) measurements** are producing the sampling values of a physical variable, denoted here as $r_{BI}(\nu, i, e, g)$ and called **bidirectional reflectance**, a concept different from but often mixed with BRDF. Integration of BRDF over all view angles gives the directional-hemispherical reflectance (DHR), r_{dh}, for given illumination angle, referred as **black-sky albedo** (see "MODIS Reflectance Products") derived from measurements by atmospheric corrections. Subsequent integration of DHR over all illumination angles gives the bihemispherical reflectance (BHR) referred as **white-sky albedo** as well, which is a measurable quantity. The **blue-sky albedo** can be derived for given ratio of the directional to diffuse radiation power, neglecting multiple scattering effects. These albedo products are used in terrestrial environment.

In the case of telescopic observations and in several satellite and airborne systems or even field measurements, often **unidirectional observations** are carried out; therefore, the irradiance or the incoming radiance cannot be measured at the level of reflecting surface, but estimated only using several BRDF-models, most often the **Lambertian model** treating diffuse radiation as isotropic scattering. Actually, the theoretical BRDF value of an isotropically scattering ideal surface can be used as normalization factor. Normalization of the true BRDF can be introduced, e.g., using the same geometry as in the target measurement, resulting in the **concept of reflectance factor**. The **bidirectional reflectance factor** $R_{BI}(\nu, i, e, g)$, abbreviated as usual as **BRF**, results from the bidirectional reflectance specially for the Sun's directional illumination as

$$R_{BI}(\nu, i, e, g) = r_{BI}(\nu, i, e, g)/(\cos(i)/\pi),$$

where the reflectance of the perfectly diffuse (isotropic) surface is $\cos(i)/\pi$ (Hapke 2012).

The directional-hemispherical reflectance of an isotropically scattering surface is

$$r_{dh} = I/F = A_L \cos(i)/\pi$$

where I is the reflected radiance (brightness), F is the (solar) irradiance, and A_L is called the **Lambertian albedo**, which is the **directional-hemispherical reflectance factor** of an isotropically scattering surface. Lambert(ian) albedo refers to radiation scattered isotropically (in all directions; from a Lambertian surface), irrespective of the incidence angle. It characterizes the material's albedo regardless of its geometry.

Normalization can be carried out with the theoretical reflectance value of an ideally diffuse surface with the illumination angle $i = 0$, rather than with the same illumination angle of the target. This quantity being used extensively is called **bidirectional radiance factor**, RADF(ν, i, e, g), a similar quantity as BRF (Hapke 1981):

$$\mathrm{RADF}(\nu, i, e, g) = r_{BI}(\nu, i, e, g)/(1/\pi),$$

Note that in planetology the factor of π is often omitted, and RADF ≈ r_{BI}(ν, i, e, g) = I/F is referred as radiance factor. It is not correct, the term so defined is only proportional to it (Thomas 2005).

The **normal albedo** is the radiance factor at $g = 0$ phase angle and at $i = e$:

$$A_n = r_{BI}(\nu, e, e, 0)/(1/\pi)$$

The dependence of viewing geometry is expressed by the **photometric function**, f(i,e,g), in connection with the brightness (radiance) values observed at fixed "e" and varying "i" and "g," after normalization (see "Reflectance Factors"):

$$\begin{aligned} f(\nu, i, e, g) &= r_{BI}(\nu, i, e, g)/r_{BI}(\nu, e, e, 0) \\ &= r_{BI}(\nu, i, e, g)/A_n \end{aligned}$$

The definition of radiance factor can be based on $r_{dh} = I/F$, denoted as r(ν, i, e, g) given as

$$r(\nu, i, e, g) = \pi I/F$$

In this case the formal definition of phase function does not change, so that

$$r(\nu, i, e, g) = A_n f(\nu, i, e, g).$$

Calculation of albedo for planetary bodies. Albedo is generally calculated starting with the *radiance factor* r of the planet: $r(\nu, i, e, g) = \pi I/F$ (Fig. 3).

Several authors derived semiempirical photometric functions from physical laws. The most widely used are the Hapke (1981) and Shkuratov (Shkuratov et al. 1999) functions, as they well reproduce both laboratory and planetary data. Nevertheless, McEwen (1991) demonstrated that if not used near the limb or terminator, simpler functions, such as that of Lambert and Minnaert (Minnaert 1941), show negligible deviations from the more complex Hapke and Shkuratov models.

Using the semiempirical expression of Minnaert for the photometric function, the radiance factor can be written as

$$\begin{aligned} r(\nu, i, e, g) &= B_0(\nu, g)(\cos i)^{k(\nu, g)}(\cos e)^{k(\nu, g)-1} \\ &= B_0(\nu, 0) f_{Minn}(\nu, i, e, g) \end{aligned} \quad (1)$$

where f_{Minn} is the Minnaert photometric function and B_0(ν, g) and k(ν, g) are the Minnaert empirical coefficients. B_0 equals A_N at $g = 0$, while k is related to the *limb-darkening* effect. Indeed, at zero-phase angle, the values 0, ½, and 1 for the k parameter correspond to opposition limb effects of cosine brightening, uniform disk brightness, and the cosine darkening brightness of a perfect Lambert surface, respectively. In the visible spectral range, the full Moon has $k = 0.5$ (uniform disk brightness) (Harris 1961). For $k = 1$, the Minnaert expression (1) reduces to

$$r(\nu, i, e, g) = A_L(\nu, g) \cos i \quad (2)$$

where A_L is the Lambert albedo. Expression (2) is the Lambert model, or the *cosine* model. This

expression provides an easier method of deriving albedo from surface measurements.

The Minnaert model also allows the derivation of information about the roughness degree of the observed surfaces, starting from the evaluation of the limb-darkening parameter k.

It has been demonstrated by several authors (Veverka et al. 1978a, b, 1986; Goguen 1981; McEwen 1991; Erard et al. 1994; Esposito et al. 2007) that the Minnaert model well describes the scattering properties of most particulate materials and planetary surfaces, especially at small-phase angles (<40°). The model cannot be used with observations of the limb and at the terminator of a planet and with mirror-like surfaces.

Veverka et al. (1978a) observed experimentally that *k* is related to multiple scattering as well as albedo and texture/roughness, especially for bright materials. They also demonstrated that for phase angles close to zero and surfaces with similar texture and roughness, the Minnaert parameters are linearly related with k, increasing as B_0 increases (see also Esposito et al. 2007). The limb-darkening parameter varies with the wavelength of the detected radiance. Generally, in the near IR, k varies from ~0.5 to ~1 going from very dark to bright planetary surfaces (De Grenier and Pinet 1995; Erard et al. 1994; Esposito et al. 2007). This is due to the increased contribution of multiple scattering on the radiance factor when the albedo increases. In the visible wavelength range, the limb-darkening parameter k is generally independent on surface albedo and for Mars is ~0.6 (De Grenier and Pinet 1995). This is due to the negligible contribution of multiple scattering at these wavelengths (dominance of single scattering processes). Esposito et al. 2007 produced a map of the Minnaert and Lambert albedo (Fig. 4) and of the geographical distribution of the limb-darkening parameter *k* over the surface of Mars, starting from the data obtained by the Short Wavelength Channel of the Planetary Fourier Spectrometer (PFS) on board Mars Express spacecraft (Fig. 5). This *k* map provides a relative granulometry map of the Martian surface and confirms the association of higher values of k with the fine-grained and high-albedo terrains and lower values with rougher and low-albedo material.

Formation

Albedo features seen in identically illuminated surfaces (Helfenstein and Wilson 1985) indicate material units that are horizontally distinct, e.g., in the following:

(1) Composition (e.g., dark basalt, bright frost)
(2) Physical properties: particle size (e.g., dust vs. sand), macroscale roughness, and porosity, these properties may also affect radar backscatter and thermal infrared emission; (▶ radar features, ▶ dust devil track, ▶ fine ejecta halo), crystal structure (e.g., due to weathering), due to e.g.,
(3) Emplacement, modification, and age (e.g., due to solar radiation, impact comminution)

Regional Variations

Mercury

Mercury has circular ▶ high reflectance plains, which are interpreted as volcanic plains (e.g., Prockter et al. 2010) similar to lunar maria.

Venus

Surface (clear-sky) albedo is not known for Venus, because its surface cannot be investigated by optical remote sensing due to its optically opaque atmosphere, which can be only penetrated by radar (▶ radar feature).

Moon

(▶ Mare, volcanic, ▶ swirl) (Fig. 6). Low-albedo regions (at 750 nm) are interpreted as titanium-rich dark mare lavas and mantle deposits or mature mare soils. Dark patches are thought to be produced by explosive volcanic activity (▶ dark mantling deposit, regional, ▶ dark mantling deposit, annnular, ▶ dark/bright halo pit), except for smaller, impact-related ▶ dark halo craters.

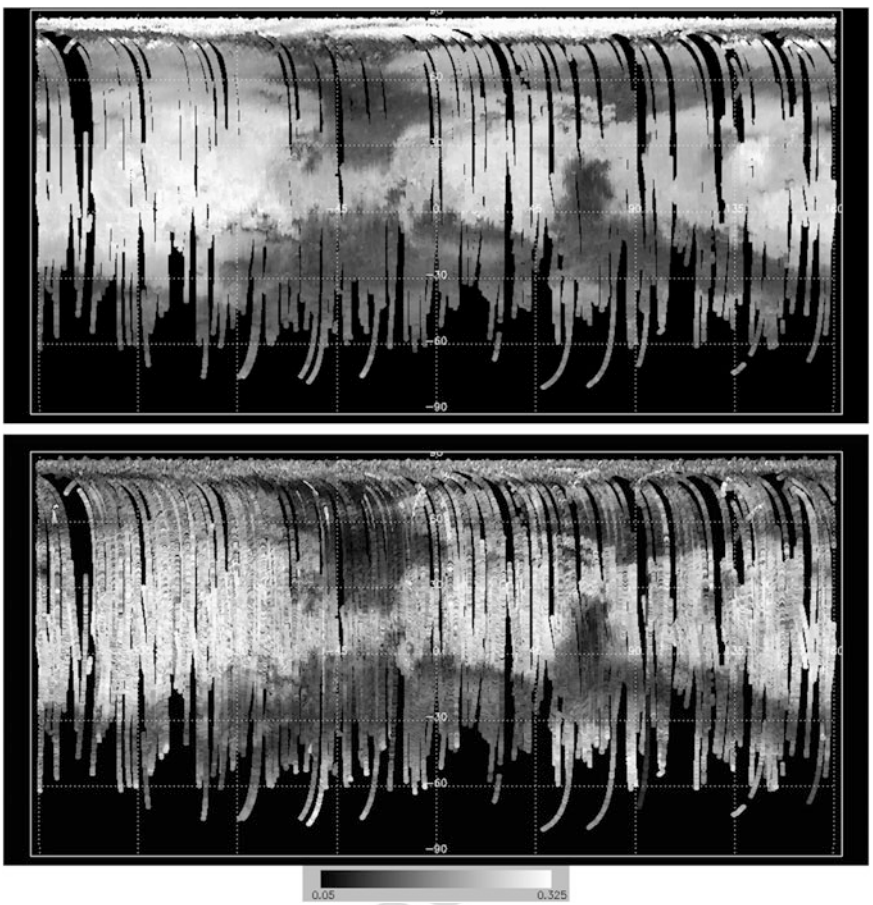

Albedo Feature, Fig. 4 Lambert albedo map obtained from PFS/MEX at 7,030 cm-1 (*bottom panel*), compared with TES/MGS albedo (*top panel*). The *top panel* has been extracted from the full resolved albedo map acquired by the spectrometer TES at a resolution of 8° per pixel by considering only the pixels corresponding to geographical points observed by PFS (Esposito et al. 2007)

Bright regions are believed to be immature soils on bright ejecta blankets of fresh impact craters or are rich in anorthosite (and poor in iron). The brightest area of the Moon is at the fresh, rayed Giordano Bruno crater and the rayless Sharonov crater which likely exposes crustal anorthosite (McEwen and Robinson 1995).

Mars

The disk of Mars is dominated by three surface albedo domains: (1) dark, (2) orange-red bright, and (3) white bright (at polar latitudes) (Fig. 7). On frost-free surfaces, low albedo correspond to high thermal inertia materials dominated by mafic particulate materials ranging from 0.1 mm to 1 cm, rather than bedrock (Ruff and Christensen 2002) (▶ dark deposits, Mars). High albedo corresponds to low inertia materials (dust particles of 2–40 μm) (Fig. 8). Thermal inertia is the ability of a material to conduct and store heat, e.g., during the day, and reradiate it during the night (▶ aeolian dust deposit).

The albedo contrast of Mars is greatest in red color (centered near 0.6 μm) (Barlow 2008, p. 73).

Albedo Classes of Mars and Their Interpretation

Note that when referring to albedo features, the classical albedo nomenclature is used: high- and low-albedo regions on Mars are defined as those

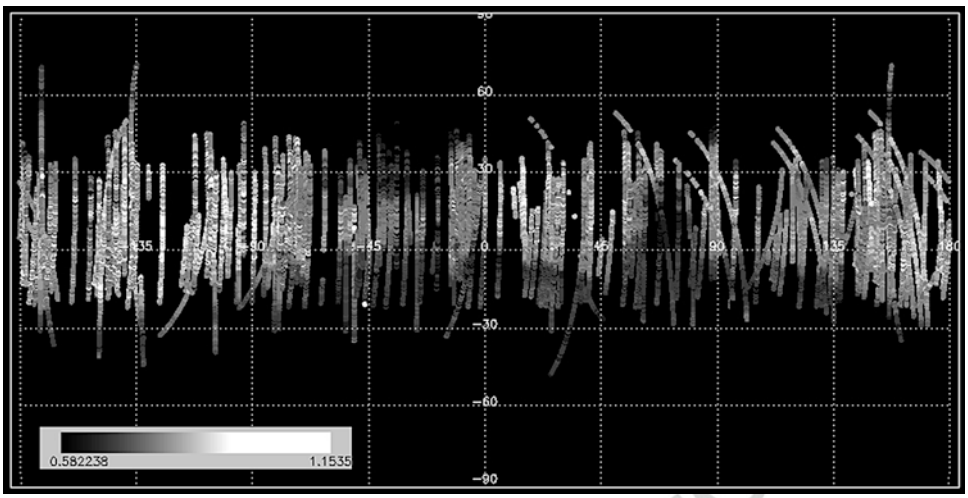

Albedo Feature, Fig. 5 Limb-darkening parameter maps, obtained at 7,030 cm-1 from PFS/MEX measurements (Esposito et al. 2007)

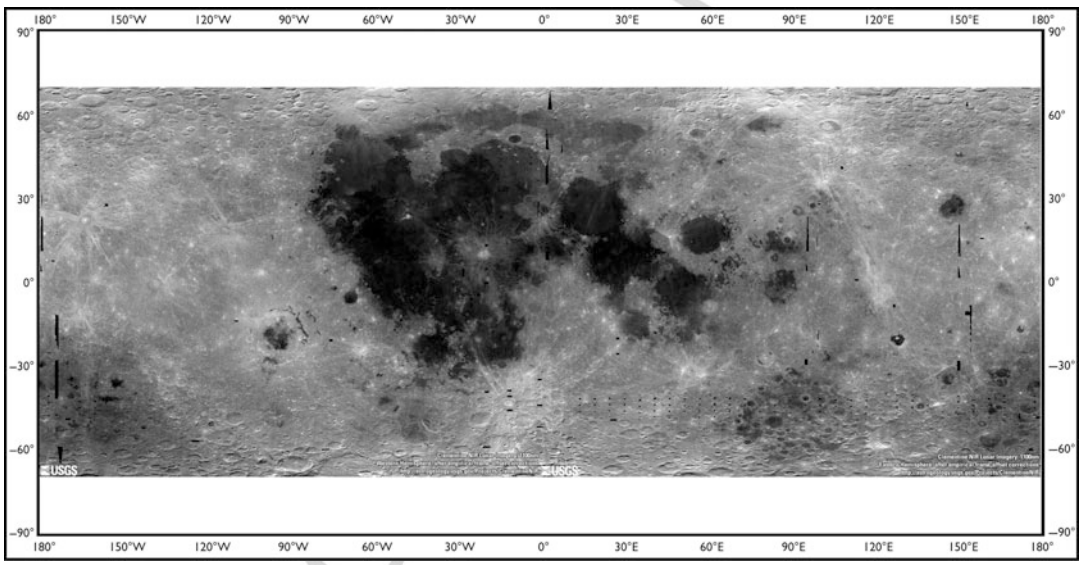

Albedo Feature, Fig. 6 Clementine NIR albedo mosaic of the Moon (70°N–70°S latitudes) (USNRL/BMDO/USGS)

higher and lower, respectively, than 0.2 (Ruff and Christensen 2002) or 0.15 as measured by MGS-TES (Rogers et al. 2007).

(1) Very high albedo: areas of seasonal frost and perennial polar ice caps.
(2) High albedo: associated with a thick (>1 m) layer of fine-grained particles (2–40 μm) (dust) (Ruff and Christensen 2002). These are also known as three low thermal inertia regions (Fenton et al. 2007): Tharsis/Amazonis, Arabia, and Elysium/Isidis (albedo: 0.27–0.30) (Christensen 1988). For comparison, the "light-toned" sedimentary outcrop of White Rock has an albedo of 0.18 (▶ light toned deposit).
(3) Low albedo: most Martian low-albedo features correspond to areas covered by bedrock outcrops or coarse grains (710–1,000 μm) of

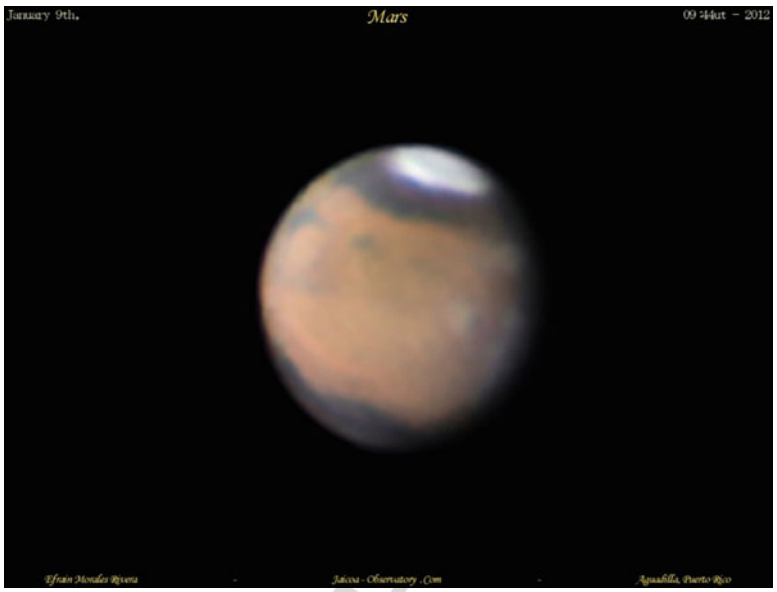

Albedo Feature, Fig. 7 Three units with distinct albedos on Mars, as seen from Earth (Photo by Efrain Morales, Jaicoa Observatory, Jan 9, 2002)

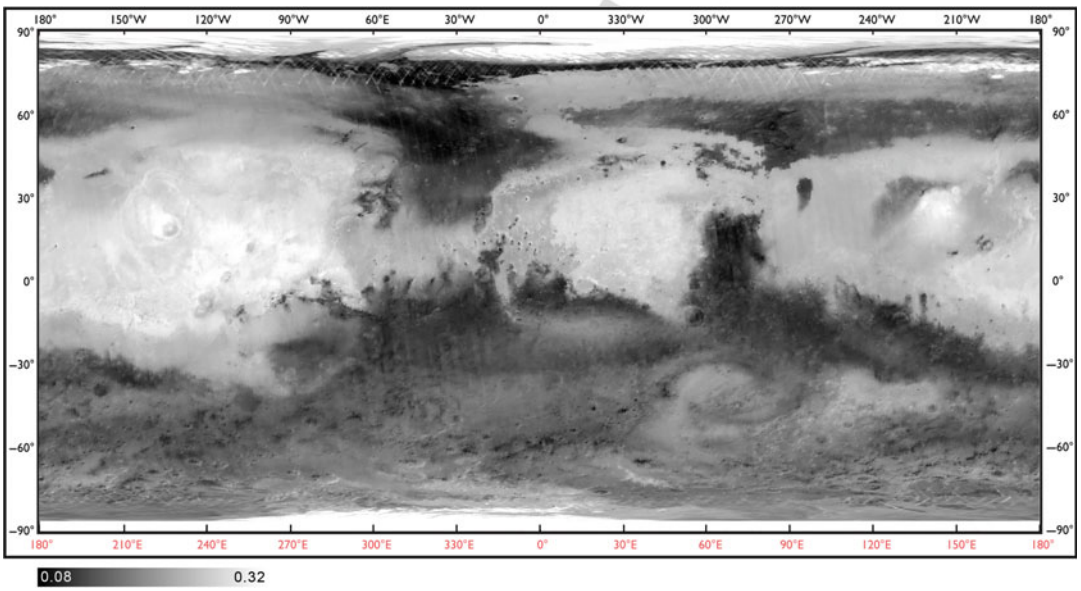

Albedo Feature, Fig. 8 Regional albedo variations on Mars, MGS-TES (Christensen et al. 2001). Values range from 0.08 (shown in *black*) to 0.32 (shown in *white*). http://www.mars.asu.edu/data/tes_albedo/ (NASA/JPL/ASU)

basaltic and andesitic materials (Ruff and Christensen 2002). Typically, dust-free regions of Mars include Syrtis Major (a basaltic volcano) and Mare Acidalium, the Southern Tropical Dark Band (Mare Cimmerium–Mare Sirenum), and the Southern High-Latitude Band (Mare Chronium–Mare Australis) (Geissler 2005).

(4) Intermediate albedo (~0.15–0.19) (Rogers et al. 2007): on Mars, an intermediate albedo type is also observed between dark and bright (intermediate values exist for both albedo and thermal inertia) which is not a transitional

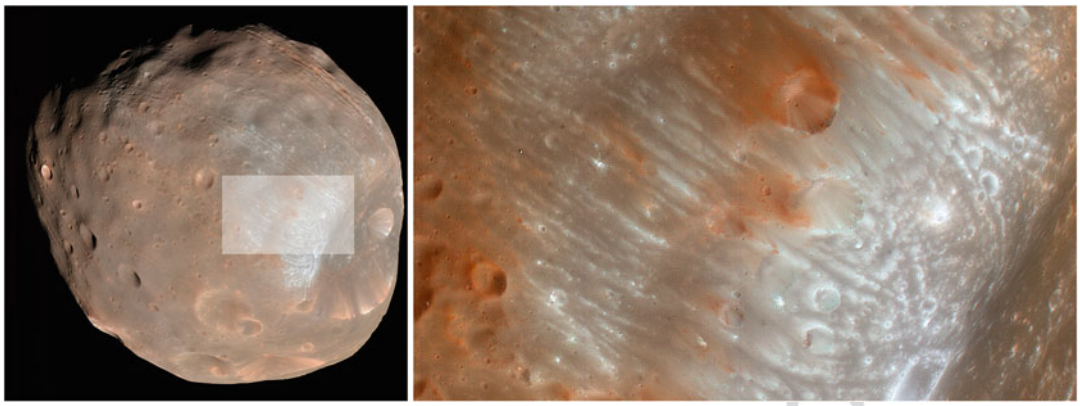

Albedo Feature, Fig. 9 Phobos albedo units. HiRISE PSP_007769_9010 (NASA/JPL/UA)

type, but likely corresponds to well-indurated duricrust (Christensen et al. 2001 and references therein).

(5) Other albedo features: dark terrains, particularly at high latitudes, are dominated by ► dust devil tracks where bright dust have been removed from the surface. Dark (mafic) sand covers large areas in the northern circumpolar ► erg and occurs in smaller patches in intracrater dune fields. Exposures of subsurface ice and underlying dark material in fresh impact craters produce small high- and low-albedo spots (► splotch), respectively. ► Wind streaks may appear darker or brighter than their surroundings. The southern seasonal polar cap displays a distinct low-albedo area termed ► Cryptic Region. The seasonal cap hosts various local scale seasonal ► dark dune features.

Phobos

Is not homogeneous and consists of a bluer and redder unit (Fig. 9) (unlike Deimos). The bluer material is draped over the south-eastern rim of Stickney crater and is thought to be relatively thin (Thomas et al. 2011). According to the dynamic dust model, the blue markings are produced by horizontal wind-like motion of dust particles induced by electrostatic levitation. Solar UV-radiated slope surfaces are positively charged: high energy UV radiation produces photoelectrons that escape (emit/detach) from the surface and thus charge the dust positively. This occurs only when the electrostatic force is larger than gravity and cohesive force together. Dust particles accelerate and may follow a ballistic trajectory. The night side (or shadowed area) is negatively charged, because without UV radiation, there are no photoelectrons produced. Also, the emitted electrons may be deposited on the night side (Zakharov 2012). This dust migration may produce a dust belt (ring) around Phobos and a dust torus around Deimos (Krivov and Hamilton 1997) (► dust pond).

Gaspra

(Main belt asteroid): there are bluer terrains at the high slope angle surface units and fresh craters, where the regolith is interpreted to be younger and less weathered than at other locations (Clark et al. 2001).

Io

Distinctly colored plains on Io occur in geographically constrained distributions: the two most extensive units are red-brown plains (8.6 % of surface), which occur $>\pm 30^\circ$ latitudes, and white plains (6.9 % of surface), mostly in the equatorial anti-Jovian region ($<\pm 30^\circ$ latitudes, 90–230°W). Red-brown plains result from long-term accumulation of ► red diffuse deposits and are interpreted to be the result of alteration from condensed sulfur gas induced by exposure to radiation coming in from the poles. White plains accumulated white diffuse material that is interpreted as condensed SO_2 (coarse- to

moderate-sized grains of SO_2 snow and frost) and its contaminants and possibly indicate regions of cold traps (Williams et al. 2011 and references therein).

Europa

Low-resolution Voyager imagery showed smaller and larger darks spots and linear features. Small spots were named ▶ lenticulae, larger ones, ▶ maculae. Collections of uneven splotches were informally termed ▶ mottled terrain. Linear features were named ▶ lineae, of which one specific type was termed ▶ triple band. Higher-resolution Galileo images revealed the true morphology of these features. Lenticulae and maculae (albedo features) are both a type of ▶ chaotic terrain (topographic feature), and some were officially named ▶ chaos. Triple bands (albedo feature) were revealed to be ▶ double ridges (topographic feature) after higher-resolution, low-sun images became available (Greenberg 2008, p. 20; Fig. 2). The descriptor term ▶ regio is used for bright plains crisscrossed by ridges (e.g., Falga Regio) and chaos-like darker regions (mottled terrains) (e.g., Dyfed Regio) (Doggett et al. 2009).

One of the darkest and reddest features on Europa is Castalia Macula (informally known as "the dark spot") (Prockter and Schenk 2005) which is interpreted to be a young structure.

For hemispheric albedo features of Europa, see ▶ Albedo/Color Dichotomy.

For regional scale albedo features of **Ganymede** see ▶ Albedo/Color Dichotomy.

For hemispheric albedo features of the **mid-sized Saturnian satellites**, see ▶ Albedo/Color Dichotomy.

Enceladus

The visual geometric albedo of Enceladus is 1.4, which makes it one of the brightest satellites in the Solar System. Its reflectance spectrum is dominated by pure water ice. The surface may be coated by particles from Saturn's E ring, whose impacts comminuted the regolith into fine-grained bright material, combined with a fallout of particles from venting or geyser-like activity. The brightest of the ▶ bright plains occurs in the south polar terrain, in the ▶ Tiger stripes region. These plains are 10 % brighter than the average reflectivity of Enceladus possibly due to particle fallout and also display the greatest albedo contrast (20 %) between the darker, coarser-grained stripes and the plains (Porco et al. 2006).

Dione, Rhea

See ▶ Wispy Markings.

Titan

Titan appears gray at visible wavelengths (Vixie et al. 2012). On Titan's surface, low- and high-albedo regions can be distinguished (Fig. 10). These units have sharp contact in several locations (e.g., in Western Xanadu) (Fig. 11).

The following models have been put forward to explain albedo variations (Porco et al. 2005 and references therein, Langhans et al. 2012 and references therein):

(1) Dark regions are liquid or solid hydrocarbons precipitated from the atmosphere, while bright regions are water-ice bedrock outcrops.
(2) Dark areas are hydrocarbon liquids, whereas bright ones are ethane mist overlying the liquid. This theory requires the change of most surface patterns that are not confirmed by observations. Observations show that bright regions are at a higher topographical level than dark ones.
(3) Dark areas are composed of an easily deformable, probably organic material precipitated from the atmosphere. A thin, brittle crust of bright material overlies it and exposes dark regions when pulled apart.

Spectral mapping by Cassini's Visible and Infrared Mapping Spectrometer, covering a spectral range from 0.35 to 5.2 microns, could distinguish three spectral surface units that may reflect differences in composition or grain size.

(1) Bright unit forms islands and large continents (e.g., Xanadu), interpreted to be older and elevated as compared to dark surfaces.

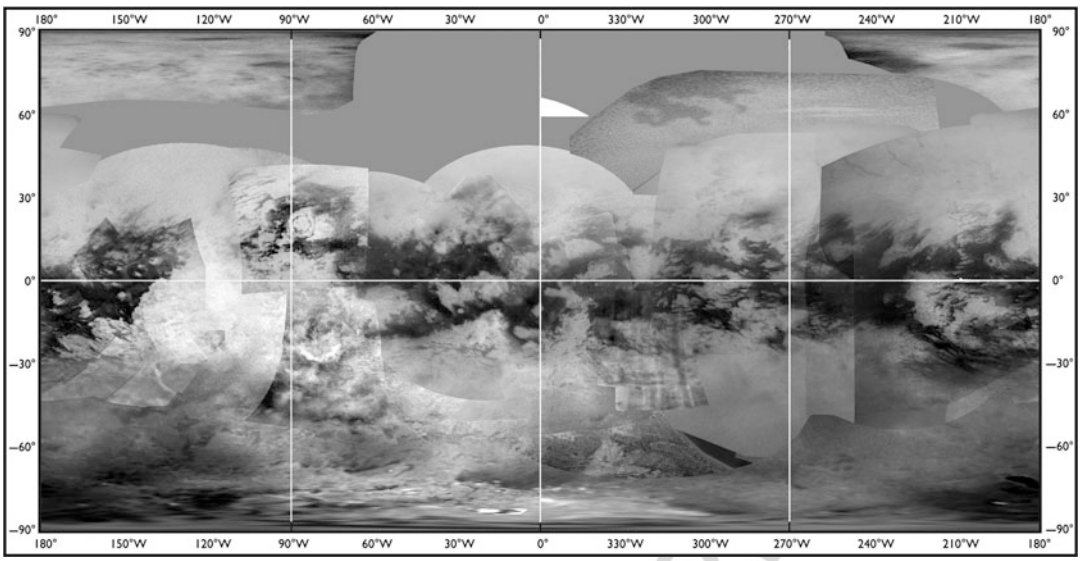

Albedo Feature, Fig. 10 938-nm methane window albedo map of Titan. Cassini ISS mosaic, February 2009 (NASA/JPL/SSI)

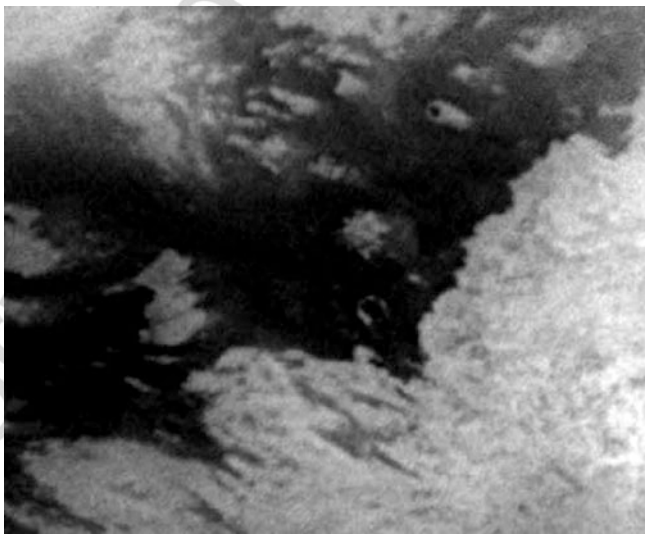

Albedo Feature, Fig. 11 The boundary between Shangri-La (*dark*) and Xanadu (*bright*, *right*), Titan (Porco et al. 2005). Cassini ISS mosaic (NASA/JPL/SSI)

(2) Dark brown unit broadly correlates with Titan's equatorial dune fields.
(3) Dark blue unit often occurs at the eastern boundaries of bright terrains and is thought to have higher water-ice content compared to the other surface units.

See also "► Mid-latitude Dark Linear Feature."

Significance

Monitoring albedo variations with time allows for the study of the following important aspects of terrains: (1) resurfacing phenomena and redistribution of dust on the surface, (2) the nature of the surface materials in terms of granulometry, and (3) the contribution of surface–atmosphere interaction to geologic and climatic evolution of the planet (indeed albedo changes could affect

solar heating and the global circulation of winds across the planet).

Changes in surface albedo indicate active surface processes. Regolith maturity (which also involves compositional changes) can be inferred from albedo. Temporal, reoccurring albedo changes might imply seasonal changes. Albedo changes affect the absorption of solar energy by the surface and impact the global climate and circulation of winds (Fenton et al. 2007; Geissler et al. 2008). Simulations show that a runaway ice-albedo mechanism can result in an ice-covered Earth (Poulsen 2003).

Differentiation of surface albedo features from atmospheric features is essential in photogeological interpretation of low-resolution (telescopic or spacecraft imagery) observations. While highly variable albedo features are likely associated with atmospheric phenomena (i.e., clouds), permanent albedo patterns more probably represent surface features. Recurrent albedo features are likely associated with seasonal changes on the surface (e.g., extension of the polar cap) or near-surface (e.g., high-albedo fogs in Hellas, Mars (Leonard and Tanaka 2001)) or atmospheric features related to topography (e.g., orographic clouds near Tharsis Montes, Mars), which rotate with the diurnal rotation of the planet (Beish 1999). Quasi-permanent albedo features may be associated with atmospheric phenomena (e.g., The Great Red Spot of Jupiter). Reappearance of confirmed surface albedo patterns can be used to determine rotation period (Beer and Mädler 1830; Clerke 1885[2010], p. 320). This is also essential for establishing a surface-bound coordinate (longitude) system.

Surface features may be misinterpreted as atmospheric features and vice versa. Schröter interpreted dark albedo features of Mars as relatively stable clouds influenced by underlying aerographical features (Clerke 1885[2010], p. 320). The Great Red Spot was thought to be reflections from an active volcano or a topographic feature fixed to the planet as suggested by N. Green in 1887 (Rogers 1995, p. 255). The apparent color of Titan was initially theorized to be the color of the visible surface below a thin atmosphere (McCord et al. 1971) and determined to be the color of an optically thick atmosphere by polarimetric measurements (Veverka 1973).

Terrestrial Analog

Earth's surface has three major albedo domains: (1) low-albedo oceans and seas, (2) intermediate-albedo continents, and (3) high-albedo seasonal or perennial snow and/or ice blankets and sea ice (Fig. 12). Ocean Surface Albedo (OSA) is "the ratio of the upwelling to down-welling solar irradiance (flux) at the air-sea boundary." Clear-sky (cloudless) ocean albedo varies between 0.03 and 0.4 depending on solar zenith angle. Its value greatly depends on wind at low sun (Jin et al. 2004).

Alteration

Albedo features may change their albedo and shape on seasonal and decadal time scales. Changes in albedo are now believed to be generated by erosion and deposition of the bright Martian dust by the wind and not by the displacement of mobile dark sand (Geissler and Mukherjee 2010; Geissler 2004, 2005). In some places, dust is stripped away episodically or albedo boundaries advance gradually at speeds of up to tens of kilometers per Martian year (Geissler and Mukherjee 2010; Fig. 13a).

Temporal behavior of albedo features has been classified into the following subtypes:

(a) By Beish (2011): (1) seasonal and (2) secular
(b) By Geissler and Mukherjee (2010): (1) features showing gradual changes, (2) features showing episodic changes that typically took place during the perihelion season, and (3) features showing changes on a quasi-continuous basis (e.g., Solis Lacus)

On the Moon, both high-albedo fresh impact ejecta (albedo ca. 0.15–0.17) and low-albedo fresh maria (0.8–0.11) surfaces change their albedo with time, eventually reaching the average

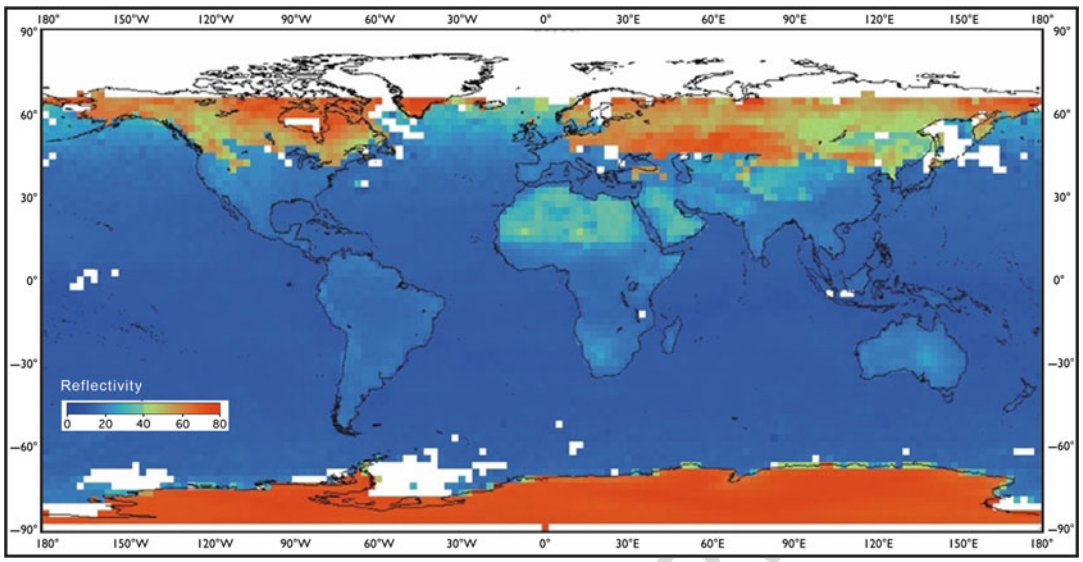

Albedo Feature, Fig. 12 Clear-sky (cloudless) albedo variations on Earth for January 1987 (northern winter). *White dots*: no data (Budikova 2013). Earth Radiation Budget Experiment (NASA)

albedo of mature highlands (0.11) (Wood 2003). With time, surface albedo decreases in visible to near-IR: mafic absorption features are attenuated, while a strong positive slope is introduced, causing spectral reddening. Lunar albedo changes are due to space weathering (the bombardment by solar wind ions and micrometeorites) (Cassidy and Hapke 1975) which creates amorphous coatings on grain surfaces and tiny blebs of metallic (nanophase) iron (Kramer et al. 2011).

On Mars, low-albedo materials exhibit the least amount of effects from alteration. Cerberus is a dark feature that almost disappeared under a newly emplaced dust mantle between 1982 and 1995 (between Viking and MGS observations) (Geissler 2004; Lee et al. 1996; Fig. 13b). Solis Lacus (in Solis Planum) shows dramatic seasonal and secular variations; this is an area of bright and dark wind streaks. Seasonal changes are explained by the following cyclical mechanism: during early southern summer, dust is removed by dust storms which results in the dark Solis Lacus feature. Following the dust storm season, in late summer, enhanced deposition occurs in the lee sides, forming bright streaks. Later, dust is deposited from the air over the entire region that decreases the contrasts of albedo features (Lee 1985).

Albedo variations during a dust storm cannot be always imputed to real surface albedo changes, as the augmented number of dust particles suspended in the atmosphere tends to raise the albedo value measured by orbiting instruments. Zinzi et al. (2010) demonstrated that using the Dust Cover Index (DCI) developed by Ruff and Christensen (2002), it is possible to correct data from this bias. Zinzi pointed out that the dust transported and deposited by a storm does not significantly affect high-albedo areas, whereas major changes of surface albedo are registered for dark regions.

Using TES data collected between 1999 and 2005, Zinzi et al. (2010) demonstrated that the surface albedo of Syrtis Major raised to an intermediate value (i.e., roughly 0.2) for months after a dust storm has ended. The atmospheric dust opacity returned lower than 0.2 on June 2002, whereas the surface albedo returned to the typical value of 0.12 only on March 2003 (Zinzi et al. 2010; Fig. 14), thus demonstrating that the dust deposited on the ground during the storm remained well after the end of the storm there, effectively changing the surface albedo.

On Europa, many features, including bands, appear to brighten with age. The youngest forms

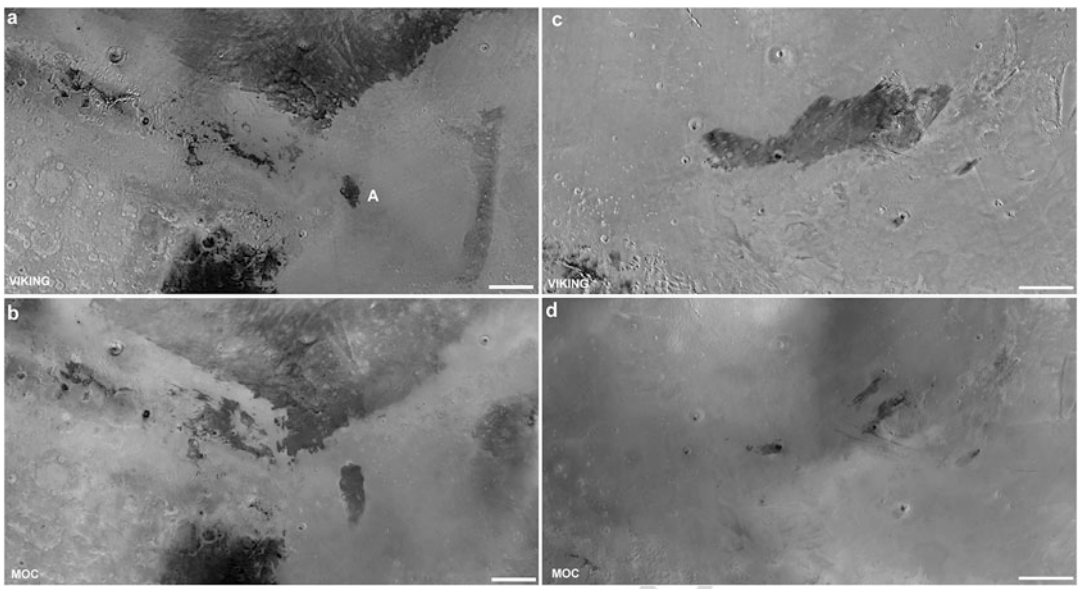

Albedo Feature, Fig. 13 Surface changes over 20 Earth years. (**a, b**) Changes in Utopia Planitia. The isolated dark patch (A) is Alcyonius, at 33°N, 94°E. Scale bar ~500 km (Geissler et al. 2008). (**c, d**). Surface changes in Cerberus, Mars. Scale bar ~300 km (Geissler 2005). (**a**, **c**): Viking; (**b**, **d**): MOC (NASA/JPL/MSSS)

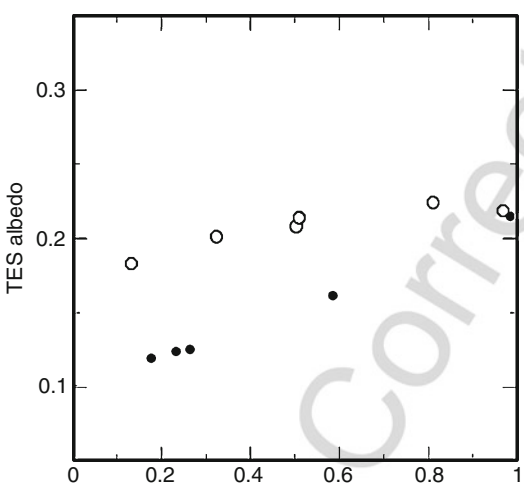

Albedo Feature, Fig. 14 Syrtis major albedo observations before and after a dust storm showing two different trends with atmospheric opacity. *Black dots* are the before-storm observations, while *white dots* are after-storm ones. TES albedo: albedo from MGS Thermal Emission Spectrometer; τ: opacity (After Zinzi et al. 2010) (Reprinted from Icarus, 208, Zinzi A, Palomba E, Rinaldi G, D'Amore M, Effect of atmospheric dust loading on Martian albedo features, 590–597. Copyright (2010), with permission from Elsevier)

are commonly of lower albedo than their surroundings, while older bands show little or no albedo contrast relative to their surroundings (Collins et al. 2010). The oldest surfaces, ridged plains, have the highest albedo. Brightening may be due to frost deposition or chemical alteration (Prockter and Schenk 2005). Crater rays are usually bright and darken with age.

History of Investigation

The lunar brightness scales. Early selenographers used a three-degree scale for brightness values (Beer and Madler 1838). The 10° scale of brightness values was established by Schröter (1791, 61§24) to help visual observations of the Moon. This brightness scale was applied and refined by late-nineteenth–early-twentieth-century observers (e.g., Lohrmann, Beer and Mädler, Elger). In the 10° scale, "zero value corresponds to the shadow which is projected by the mountains. The first three degrees may be denominated grey, the fourth and fifth, light grey, the sixth and seventh, white, and the last three, shining white. The 1st,

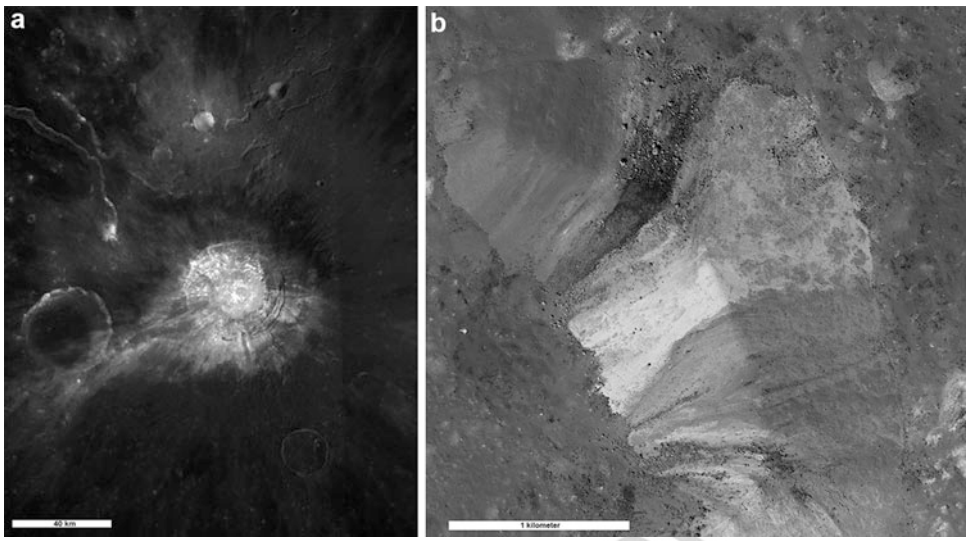

Albedo Feature, Fig. 15 Aristarchus crater, the brightest spot of the Moon. (**a**) Clementine UVVIS 750 nm mosaic (USNRL/BMDO/USGS), (**b**) Bright material of Aristarchus central peak, LROC NAC mosaic (NASA/GSFC/ASU)

9th, and 10th degrees are found only on small parts of some spots. It is in the craters, and in the annular mountains, that we find the last three degrees of brightness. There is only one annular mountain, viz. Aristarchus (Fig. 15), and one point in Werner which reach the 10th and highest degree of illumination" (Beer and Madler 1838).

Elger (1895) added more details: "The most brilliant object on the surface is the central peak of the ring-plain Aristarchus, the darkest the floor of Grimaldi, or perhaps a portion of that of the neighbouring Riccioli. Between these extremes, there is every gradation of tone."

Neison (1876) referred to brightness as "the general tint."

The lunar brightness scale values were difficult to correlate to brightness values of known terrestrial materials. John Herschel maintained that "the actual illumination of the lunar surface is not much superior to that of weathered sandstone rock in full sunshine." "I have," Herschel explained further, "frequently compared the moon setting behind the grey perpendicular facade of the Table Mountain, illuminated by the sun just risen in the opposite quarter of the horizon, when it has been scarcely distinguishable in brightness from the rock in contact with it" (Herschel 1893).

Elger (1895) remarked that "Proctor, discussing this question on the basis of Zollner's experiments respecting the light reflected by various substances, concludes that the dark area just mentioned must be notably darker than the dark grey syenite which figures in his tables, while the floor of Aristarchus is as white as newly fallen snow."

The 10° scale was standardized by the Selenographical Society and the *Selenographical Journal* provided a list of lunar features for each value (Elger 1895). They were correlated to albedo values by Fessenkov (1962; Table 1).

In the 1920s, photoelectric photometry provided objective measurements of the albedo of any selected spots, and modern CCD detectors are able to measure the albedo of broader areas. A spectrometer is a device measuring properties of the electromagnetic radiance.

While the brightness scale was specifically designed for lunar observations, having values from the darkest, shadowed areas (0°) to the brightest spot of the near side of the Moon (10°), albedo values measure the reflectivity of the surface from 0 (incident light is completely absorbed) to 1.0 (100 % of incident light is reflected) (Wood 2007).

Albedo Feature, Table 1 The lunar brightness scale, after Elger 1895 and Fessenkov (1962)

Brightness scale (degree)	Selenographical Society (Elger 1895)	Feature, *Selenographical Journal* (Elger 1895)	Feature, Fessenkov (1962)	Albedo, Fessenkov (1962)
0	Black/real shadow of lunar mountains	Black shadows		
1	Grayish black	Darkest portions of the floors of Grimaldi and Riccioli	Grimaldi and Riccioli floors	0.061
1.5		Interiors of Boscovich, Billy, and Zupus	Boscovich floor	0.067
2	Dark gray	Floors of Endymion, Le Monnier, Julius Caesar, Cruger, and Fourier	Julius Caesar and Endymion floors	0.074
2.5		Interiors of Azout, Vitruvius, Pitatus, Hippalus, and Marius	Pitatus and Marius floors	0.081
3	Medium gray	Interiors of Taruntius, Plinius, Theophilus, Parrot, Flamsteed, and Mercator	Taruntius, Plinius, Flamsteed, Theophilus, Mercator floors	0.088
3.5		Interiors of Hansen, Archimedes, and Mersenius	Hansen, Archimedes, and Mersenius floors	0.095
4	Yellowish gray, average light	Interiors of Manilius, Ptolemaeus, and Guerike	Ptolemaeus, Manilius, and Guericke floors	0.102
4.5		Surface round Aristillus, Sinus Medii	Aristillus environs	0.109
5	Pure light gray	Walls of Arago, Landsberg, and Bullialdus. Surface round Kepler and Archimedes	Arago, Landsberg, and Bullialdus walls, Kepler environs	0.115
5.5		Walls of Picard and Timocharis. Rays from Copernicus	Picard and Timocharis walls, rays of Copernicus	0.122
6	Light whitish gray	Walls of Macrobius, Kant, Bessel, Mosting, and Flamsteed	Macrobius, Kant, Bessel, Mösting, and Flamsteed walls	0.129
6.5		Walls of Langrenus, Theaetetus, and Lahire	Lagrange, Mons La Hire, and Theaetetus walls	0.135
7	Grayish white	Theon, Ariadaeus, Bode B, Wichmann, and Kepler	Theon Junior, Ariadaeus, Behaim, and Bode B walls	0.142
7.5		Ukert, Hortensius, Euclides	Euclides, Ukert, and Hortensius walls	0.149
8	Pure white	Walls of Godin, Bode, and Copernicus	Godin, Copernicus, and Bode walls	0.156
8.5		Walls of Proclus, Bode A, and Hipparchus C	Proclus, Bode A, and Hipparchus C walls	0.163
9	Glittering white/ Proclus	Censorinus, Dionysius, Mosting A, and Mersenius B and C	Mersenius and Mosting A walls	0.169
9.5		Interior of Aristarchus, La Peyrouse DELTA	Aristarchus interior	0.176
10	Dazzling white/ Aristarchus brightest	Central peak of Aristarchus	Aristarchus central peaks	0.183

Albedo Mapping

Earth-based telescopic observations are not capable to resolve topographic features on other planets and moons (except for our Moon), due to low resolution and the lack of discernible shadows, particularly on Mars and outer Solar System bodies, which are always observed as a full or nearly full disks from the Earth. Topographic shading is also absent in orbital images of Titan, because of the scattering of light by Titan's atmosphere (JPL 2007).

Topographic information is generally obtained from close/targeted flybys or from orbital missions. Before such data becomes available, albedo (spectro-/photometric) maps can be constructed through the following methods and sources: (1) rotation light curves, (2) light curves from mutual events (occultations, eclipses, and transits) (e.g., Pluto albedo maps, Buie et al. 1992), (3) distant (Earth-based) telescopic observations (e.g., early Mars maps or Hubble Space Telescope's albedo map of Vesta, Li et al. 2010), and (4) low-resolution spacecraft imagery from distant/nontargeted flybys (e.g., Pioneer images of the Galilean satellites, Fimmel et al. 1977, p. 180).

On Mars, Viking infrared thermal mapper (IRTM) and MGS-TES provided detailed temporal and spatial albedo information (Christensen 1988). The first digital measurements of lunar albedo were provided by Clementine at 750 nm. Today, high-resolution reflectance and emissivity spectra (hyperspectral data curves) are used for the estimation of mineralogical compositions of surface materials, instead of a single, averaged albedo value (▶ Dark deposits).

Albedo Features of Mars

Albedo and shape of features of the Martian disk as seen from the Earth have been recorded in all apparitions since the early twentieth century and still are recorded by amateur Mars observers.

Martian surface was classified into dark areas, light areas, canals, and oases (all albedo features) during much of the twentieth century. Even in 1970, Ronca proposed two possible interpretations: one based on an Earth-like Mars (in this model, albedo features corresponded to continents, ocean basins, and tectonic environments) and a second based on a Moon-like Mars (with features equivalent to the lunar maria, terrae, and rays) (Ronca 1970) (▶ dark splotch, ▶ dark deposits (Mars)).

It was observed by several astronomers in the early twentieth century that during the southern spring, albedo features darken gradually from the South towards the equator and vice versa during the northern spring. This phenomenon was called the "Wave of darkening" and was explained by the activity of vegetation during the spring, associated with the melting of the polar ice cap. In the 1960s to 1980s, several workers expressed their doubts on its existence (Kieffer 1992, p. 42), while others showed that actually a wave of brightening occurs as bright fresh dust is deposited in areas adjacent to dark features (Beish 2011).

Albedo Features (Moons of Jupiter and Saturn)

Brightness variability of the Jovian and Kronian moons has been demonstrated by Guthnick (e.g., 1906). Based on his results (See (1910)), he proposed that satellites of Jupiter and Saturn have lunar-like maria on their surfaces. Guthnick's observations could show in 1925 that the Galilean moons are tidally locked (Ulivi and Harland 2007, p. xli).

The first photoelectric photometry-based information on the Galilean moon's brightness was published by Stebbins (1927) which also confirmed synchronous rotation.

Thomas Lee suggested that the high albedo from VIS to 3.4 μm of Io is compatible with a sulfur compound (Lee 1971). The drop in the curves for Europa and Ganymede confirmed Kuiper's earlier suggestion that H2O ice is present on these satellites (▶ bright plains) (Cruikshank and Nelson 2007).

The Darkening Process

Gold (1955) proposed that the lunar surface darkens with time, as inferred from the existence of bright rays only at young craters. Optical effects of space weathering were thought to be caused by impact vitrified glass in agglutinates, and submicroscopic iron was believed to result

from impact melting of minerals whose surfaces are saturated with solar wind-transported hydrogen. However, vacuum-melted glasses are not dark. Hapke et al. (1975) suggested that the spectral effects are due to vapor condensates, which became accepted in the 2000s (Hapke 2001).

Origin of Term

The term albedo was introduced into optics by Lambert (1760). Since the illuminating light source is the Sun, which appears white for visual inspection, the portion of reflected Sun's radiation appears the whiter, the larger portion of radiation power is reflected by the surface. This is the origin of the term "albedo", construed from the Latin word "albus," meaning "white."

IAU Descriptor Term

Descriptor terms of albedo features without genetic implications include macula (dark spot), facula (bright spot), regio (large area), and linea (linear feature).

Mare and terra as descriptor terms were first applied to lunar dark and bright regions, respectively, by Langrenus in 1645. The presently used system of lunar nomenclature was introduced by Riccioli in 1651. Low-albedo regions are now known to be composed of mare materials (basaltic plains). High-albedo regions (highland terrains), used to be called terrae, are today unnamed. Several albedo features on the Moon have no corresponding topographic landform (e.g., Reiner Gamma).

The presently used system of nomenclature of both dark and bright "classical albedo features" on Mars was developed by Schiaparelli in the late nineteenth century. Additional features were identified and named by Antoniadi and Lowell at the beginning of the twentieth century, some of which were observational artifacts. About 100 of their albedo names were transferred into the names of corresponding or nearby topographic features (Coprates Canal→Coprates Chasma→Hellas→ Hellas Planitia→Syrtis Major→Syrtis Major Planum; etc.) (de Vaucouleurs et al. 1975), but about 400 have not been carried forward (Gangale and Dudley-Flores 2013).

The albedo features of Mercury were named originally by Antoniadi. Large bright regions have no descriptor term, while dark regions are termed solitudo in the nomenclature (Dollfus et al. 1978).

See Also

- Albedo Dichotomy
- Crater Ray
- Dark Deposits (Mars)
- Dark Halo Crater
- Dust Devil Track
- Lenticula
- Mare (Volcanic)
- Palimpsest
- Red Spot (Moon)
- Slope Streak
- Swirl
- Wind Streak

References

Barlow NG (2008) Mars: an introduction to its interior, surface and atmosphere. Cambridge University Press, New York

Beer W, Mädler JH (1830) Physische Beobachtungen des Mars bei seiner Opposition im September 1830. Berlin. http://reader.digitale-sammlungen.de/de/fs1/object/goToPage/bsb10060422.html?pageNo=7

Beer W, Madler JH (1838) Survey of the surface of the moon. Edinb New Philos J 25:38–67. (English translation, condensed)

Beish JD (1999) Discrete topographic and orographic clouds of Mars. Association of Lunar and Planetary Observers. http://www.alpo-astronomy.org/mars/discrete.htm

Beish JD (2011) Surface features of Mars. In: Observing the planet Mars. http://www.alpo-astronomy.org/jbeish/Observing_Mars_4.html

Budikova D (2013) Albedo. Retrieved from http://www.eoearth.org/view/article/149954

Buie MW, Tholen DJ, Horne K (1992) Albedo maps of Pluto and Charon: initial mutual events results. Icarus 97:211–227

Cassidy W, Hapke B (1975) Effects of darkening processes on surfaces of airless bodies. Icarus 25(3):371–383

Christensen PR (1988) Global albedo variations on Mars: implications for active aeolian transport, deposition and erosion. J Geophys Res 93(B7):7611–7624

Christensen PR, Bandfield JL, Hamilton VE, Ruff SW, Kieffer HH et al (2001) Mars global surveyor thermal emission spectrometer experiment: investigation description and surface science results. J Geophys Res 106(E10):23823–23871

Clark BE, Hapke B, Pieters C, Britt D (2001) Asteroid space weathering and regolith evolution. In: Bottke WF, Cellino A, Paolicchi P, Binzel RP (eds) Asteroids III. University of Arizona Press, Tucson, pp 585–599

Clerke AM (1885[2010]) A popular history of astronomy during the nineteenth century. Cambridge University Press

Coakley JA Jr (2002) Reflectance and albedo, surface. In: Holton JR, Curry JA, Pyle JA (eds): Encyclopedia of atmospheric sciences. Academic Press,1914–1923. doi:10.1016/B0-12-227090-8/00069-5

Collins GC, McKinnon WB, Moore JM, Nimmo F, Pappalardo RT, Prockter LM, Schenk PM (2010) Tectonics of the outer planet satellites. In: Schultz RA, Watters TR (eds) Planetary tectonics. Cambridge University Press, New York, pp 264–350

Cruikshank DP, Nelson RM (2007) A history of the exploration of Io. In: Lopes RMC, Spencer JR (eds) Io after Galileo: a new view of Jupiter's volcanic moon. Springer Praxis, Berlin

De Grenier M, Pinet PC (1995) Near-opposition Martian limb-darkening: quantification and implication for visible-near infrared bidirectional reflectance studies. Icarus 115:354–368

de Vaucouleurs G, Blunck J, Davies M, Dollfus A, Koval IK, Kuiper GP, Masursky G, Miyamoto S, Moroz VI, Sagan C, Smith B (1975) The new Martian nomenclature of the International Astronomical Union. Icarus 26:85–98

Doggett T, Greeley R, Figueredo P, Tanaka K (2009) Grologic stratigraphy and evolution of Eruopa's surface. In: Pappalardo RT, McKinnon WB, Khurana K (eds) Europa. University of Arizona Press, Tucson

Dollfus A, Chapman CR, Davies ME, Gingerich O, Goldstein R, Guest J, Morrison D, Smith BA (1978) IAU Nomenclature for albedo features on the planet Mercury. Icarus 34(1):210–214

Dumont M, Sirguey P, Arnaud Y, Six D (2011) Monitoring spatial and temporal variations of surface albedo on Saint Sorlin Glacier (French Alps) using terrestrial photography. Cryosphere 5:759–771

Elger TG (1895) The Moon – a full description and map of its principal physical features. George Philip & Son, London

Erard S, Mustard J, Murchie S, Bibring JP, Cerroni P, Coradini A (1994) Martian Aerosols: near-infrared spectral properties and effects on the observation of the surface. Icarus 111:317–337

Esposito F, Giuranna M, Maturilli A, Palomba E, Colangeli L, Formisano V (2007) Albedo and photometric study of Mars with the Planetary Fourier Spectrometer on-board the Mars Express mission. Icarus 186:527–546

Fenton LK, Geissler PE, Haberle RM (2007) Global warming and climate forcing by recent albedo changes on Mars. Nature 446:646–649. doi:10.1038/nature05718

Fessenkov VG (1962) Photometry of the moon. In: Kopal Z (ed) Physics and astronomy of the moon. Academic, New York

Fimmel RO, Swindell W, Burgess E (1977) Pioneer odyssey. NASA Scientific and Technical Information Office, Washington, DC

Gangale T, Dudley-Flores M (2013) Proposed additions to the cartographic database of Mars. In: Proceedings of the 26th international cartographic conference, Dresden, P2–75

Geissler PE (2004) Three decades of Martian surface changes. Lunar Planet Sci Conf XXXV, abstract #2017, Houston

Geissler P (2005) Three decades of Martian surface changes. J Geophys Res 110:E02001. doi:10.1029/2004JE002345, 23

Geissler PE, Mukherjee P (2010) Recent surface changes on Mars. American Geophysical Union, Fall meeting 2010 #P51B–1428

Geissler PE, Tornabene L, Verba C, Bridges N et al (2008) HIRISE observations of Martian albedo boundaries. Lunar Planet Sci Conf XXXIX, abstract #2352, Houston

Goguen JD (1981) A theoretical and experimental investigation of the photometric functions of particulate surfaces, PhD thesis, Cornell University, Ithaca

Gold T (1955) The lunar surface. Mon Not R Astron Soc 115:585–604

Greenberg R (2008) Unmasking Europa. Copernicus Books, New York

Guthnick P (1906) Resultate aus photometrischen Beobachtungen der sechs helleren Saturntrabanten. Astron Nachr 171(18):273–280, 4098

Hapke B (1981) Bidirectional reflectance spectroscopy: 1. Theory J Geophys Res 86(B4):3039–3054

Hapke B (2001) Space weathering from Mercury to the asteroid belt. J Geophys Res 106(E5):10039–10073

Hapke B (2012) Theory of reflectance and emittance spectroscopy, 2nd edn. Cambridge University Press, Cambridge, UK

Hapke B, Cassidy W, Wells E (1975) Effects of vapor-phase deposition processes on the optical, chemical and magnetic properties of the lunar regolith. Moon 13:339–354

Harris DL (1961) Photometry and colorimetry of planets and satellites. In: Kuiper GP, Middlehurst BM (eds) Planets and satellites. University of Chicago Press, Chicago, pp 272–342

Helfenstein P, Wilson L (1985) Photometric constraints on the emplacement and evolution of terrains on ganymede. Lunar Planet Sci XVI:339–340, Houston

Herschel JFW (1893) Outlines of astronomy. Longmans, Green and Co, London

IAU Gazetteer (2014) Gazetteer of planetary nomenclature. International Astronomical Union, Working group for planetary system nomenclature. http://planetarynames.wr.usgs.gov/

JPL (2007) Cassini Titan 052TI(T37) Mission description. Jet Propulsion Laboratory. 12 p

Jin Z, Charlock TP, Smith Jr WL, Rutledge K (2004) A parameterization of ocean surface albedo. Geophys Res Lett 31:L22301. doi:10.1029/2004GL021180.

Kieffer HH (1992) Mars. University of Arizona Press, Tucson

Kramer GY, Besse S, Dhingra D, Nettles J, Klima R et al (2011) M3 spectral analysis of lunar swirls and the link between optical maturation and surface hydroxyl formation at magnetic anomalies. J Geophys Res 116:E00G18. doi:10.1029/2010JE003729

Krivov VA, Hamilton DP (1997) Martian dust belts: waiting for discovery. Icarus 128:335–353

Lambert JH (1760) Photometria sive de mensura et gradibus luminis, colorum et umbrae. Viduae Eberhardi Klett, Augsburg

Langhans MH, Jaumann R, Stephan K et al (2012) Titan's fluvial valleys: morphology, distribution, and spectral properties. Planet Space Sci 60:34–51

Lee T (1971) Spectral albedos of the Galilean Satellites. Communications of the Lunar and Planetary Laboratory. 9(3) No. 168. The University of Arizona, pp 179–181

Lee SW (1985) Seasonal and secular variation of the SOLIS Lacus albedo feature: relation to the Martian dust-transport cycle. Lunar Planet Sci XVI:483–484, Houston

Lee SW, Wolff MJ, Janes PB, Clancy RT, Bell JF, Martin LJ (1996) HST observations of Mars: time-variable Albedo in the Cerberus region American Astronomical Society, DPS meeting #28, #02.17, Bulletin of the American Astronomical Society, vol 28. p 106

Leonard GJ, Tanaka KL (2001) Geologic map of the Hellas Region of Mars. USGS, Reston

Li J-Y, McFadden LA, Thomas PC, Mutchler MJ, Parker JW, Young EF, Russell CT, Skyes MV, Schmidt BE (2010) Photometric mapping of Asteroid (4) Vesta's southern hemisphere with Hubble Space Telescope. Icarus 208:238–251

Liang S, Strahler AH, Walthall C (1999) Retrieval of land surface albedo from satellite observation: a simulation study. J Appl Meteorol 28:712–725

Lucchitta BK, Soderblom LA, Ferguson HM (1981) Structures on Europa. Lunar Planet Sci 12B:1555–1567, Houston

McCord TB, Johnson TV, Elias JH (1971) Saturn and its satellites: narrow band spectrophotometry (0.3–1.1 μm). Astrophys J 165:413–424

McEwen AS (1991) Photometric functions for photoclinometry and other applications. Icarus 92:298–311

McEwen AS, Robinson MS (1995) Global albedo variations on the Moon: clementine 750-nm observations. Lunar Planet Sci XXVI:931–932, Houston

Minnaert M (1941) The reciprocity principle in lunar photometry. Astrophys J 93:403–410

Neison E (1876) The Moon and the condition and configuration of its surface. Longmans, Green and Co, London

Nicodemus FE, Richmond JC, Hsia JJ, Ginsberg IW, Limperis T (1977) Geometrical considerations and nomenclature for reflectance, vol 160. National Bureau of Standards Monograph, Washington, DC

Pinty B, LattanzioA MJV, Verstraete MM, Gobron N, Taberner M, Widlowski J-L, Dickinson RE, Govaerts Y (2005) Coupling diffuse sky radiation and surface Albedo. J Atmos Sci 62:2580–2591

Plescia J (2009) Appearance of lunar features under different illuminations. Lunar Networks. http://lunarnetworks.blogspot.hu/2009/10/appearance-of-lunar-features-under.html

Porco CC et al (2005) Imaging of Titan from the Cassini spacecraft. Nature 434:159–168. doi:10.1038/nature03436

Porco CC, Helfenstein P, Thomas PC, Ingersoll AP, Wisdom J, West R, Neukum G et al (2006) Cassini observes the active south pole of Enceladus. Science 311:1393–1401. doi:10.1126/science.1123013

Poulsen CJ (2003) Absence of a runaway ice-albedo feedback in the Neoproterozoic. Geology 31(6):473–476

Prockter L, Schenk PM (2005) Origin and evolution of Castalia Macula, an anomalous young depression on Europa. Icarus 177:305–326

Prockter LM, Head JW, Pappalardo RT, Senske DA, Neukum G et al (1998) Dark Terrain on Ganymede: geological mapping and interpretation of Galileo Regio at high resolution. Icarus 135:317–344

Prockter LM, Ernst CM, Denevi BW, Chapman CR et al (2010) Evidence for young volcanism on Mercury from the third MESSENGER Flyby. Science 329:668–671. doi:10.1126/science.1188186

Rogers JH (1995) The giant planet Jupiter. Cambridge University Press, New York

Rogers AD, Bandfield JL, Christensen PR (2007) Global spectral classification of Martian low-albedo regions with Mars Global Surveyor Thermal Emission Spectrometer (MGS-TES) data. J Geophys Res 112: E02004. doi:10.1029/2006JE002726

Ronca LB (1970) An introduction to the geology of Mars. Proc Geol Assoc 81(1):111–128

Ruff SW, Christensen PR (2002) Bright and dark regions on Mars: particle size and mineralogical characteristics based on Thermal Emission Spectrometer data. J Geophys Res 107(E12):5127. doi:10.1029/2001JE001580
Sagan C, Pollack JB, Veverka J (1972) Variable features on Mars: preliminary Mariner 9 television results. Icarus 17:346–372
Schröter JH (1791) Selenotopographische Fragmente. CG Fleckeinsen, Lilenthal
See TJJ (1910) The origin of the so-called craters on the Moon by the impact of satellites, and the relation of these satellite indentations to the obliquities of the planets. Publ Astron Soc Pac 22(130):13–20
Shkuratov Y, Starukhina L, Hoffmann H, Arnold G (1999) A model of spectral albedo of particulate surfaces: implications for optical properties of the Moon. Icarus 137:235–246
Stebbins J (1927) The light variations of the satellites of Jupiter and their applications to measures of the solar constant. Lick Obs Bull 13:1–11
Strugnell NC, Lucht W (2001) An algorithm to infer continental-scale Albedo from AVHRR data, land cover class, and field observations of typical BRDFs. J Clim 14:1360–1376
Thomas N (2005) Lecture 7: surface photometry. The planet, Mars. Physikalisches Institut, University, Bern. http://space.unibe.ch/staff/thomas/07_Photometry_Rev.pdf
Thomas N, Stelter R, Ivanov A, Bridges NT, Herkenhoff KE, McEwen AS (2011) Spectral heterogeneity on Phobos and Deimos: HiRISE observations and comparisons to Mars Pathfinder results. Planetary and Space Science 59(13):1281–1292
Ulivi P, Harland DM (2007) Robotic exploration of the Solar System. Part 1. Springer-Praxis, Chichester UK
Veverka J (1973) Titan: polarimetric evidence for an optically thick atmosphere. Icarus 18:657–660
Veverka J, Goguen J, Yang S, Elliot JL (1978a) Near-opposition limb darkening of solids of planetary interest. Icarus 33:368–379
Veverka J, Goguen J, Yang S, Elliot JL (1978b) Scattering of light from particulate surfaces I. A laboratory assessment of multiple-scattering effects. Icarus 34:406–414
Veverka J, Thomas P, Johnson V, Matson DL, Housen K (1986) The physical characteristics of satellite surfaces. In: Burns J, Matthews MS (eds) Satellites. University of Arizona Press, Tucson, pp 342–402
Vixie G, Barnes JW, Bow J, Le Mouélic S, Rodriguez S, Brown RH, Cerroni R, Tosi F, Buratti B, Sotin C, Filacchione G, Capaccioni F, Coradini A (2012) Mapping Titan's surface features within the visible spectrum via Cassini VIMS. Planet Space Sci 60(1):52–61
Williams DA, Keszthelyi LP, Crown DA, Yff JA, Jaeger WL, Schenk PM, Geissler PE, Becker TL (2011) Volcanism on Io: new insights from global geologic mapping. Icarus 214:91–112
Wood CA (2003) The modern moon. A personal view. Sky Publishing, Cambridge, MA
Wood CA (2007) Lunar brightness. In: Moon.wiki. http://the-moon.wikispaces.com/Brightness+of+Selected+Features
Zakharov A (2012) Dust at the Martian Moons and in the circummartian space. The meteoroid flux in the Martian satellite system. MIIGAiK MExLab workshop. Moscow, 5–6 July 012
Zinzi A, Palomba E, Rinaldi G, D'Amore M (2010) Effect of atmospheric dust loading on Martian albedo features. Icarus 208:590–597

Alcove-Channel-Apron Morphology

► Crater Wall Flow-Like Features (Moon, Asteroids)

Alcoved Valley

► Amphitheater-Headed Valley (Mars, Earth)

Aligned Boulders, Organized Boulders

► Striped Terrain

Alkane Lake

► Lacustrine Features (Titan)

Alluvial Cone

► Alluvial Fan